Tunable polar distortions and magnetism in $Gd_xLa_{1-x}PtSb$ epitaxial films

Dongxue Du,[1] Chenyu Zhang,[1] Jingrui Wei,[1] Yujia Teng,[2] Konrad T. Genser,[2] Paul M. Voyles,[1] Karin M. Rabe,[2] and Jason K. Kawasaki[1]

[1]*Materials Science and Engineering, University of Wisconsin-Madison, Madison, WI 53706*
[2]*Department of Physics and Astronomy, Rutgers University*

(Dated: June 1, 2025)

Hexagonal *ABC* intermetallics are predicted to have tunable ferroelectric, topological, and magnetic properties as a function of the polar buckling of *BC* atomic planes. We report the impact of isovalent lanthanide substitution on the buckling, structural phase transitions, and electronic and magnetic properties of $Gd_xLa_{1-x}PtSb$ films grown by molecular beam epitaxy (MBE) on c-plane sapphire substrates. The $Gd_xLa_{1-x}PtSb$ films form a solid solution from x = 0 to 1 and retain the polar hexagonal structure ($P6_3mc$) out to $x \leq 0.95$. With increasing x, the PtSb buckling increases and the out of plane lattice constant c decreases due to the lanthanide contraction. While hexagonal LaPtSb is a highly conductive polar metal, the carrier density decreases with x until an abrupt phase transition to a zero band overlap semimetal is found for cubic GdPtSb at $x = 1$. The magnetic susceptibility peaks at small but finite x, which we attribute to Ruderman–Kittel–Kasuya–Yosida (RKKY) coupling between localized $4f$ moments, whose concentration increases with x, and free carriers that decrease with x. Samples with $x \geq 0.3$ show antiferromagnetic Curie-Weiss behavior and a Neel temperature that increases with x. The $Gd_xLa_{1-x}PtSb$ system provides opportunities to dramatically alter the polar buckling and concentration of local $4f$ moments.

I. INTRODUCTION

Polar and inversion-symmetry breaking distortions are important for tuning properties of magnetic, ferroelectric, and topological materials. In particular, the polar hexagonal *ABC* intermetallics with LiGaGe-type structure are predicted to have highly tunable properties as a function of the polar buckling in the *BC* atomic planes. These properties include ferroelectricity [1], hyperferroelectricity with persistent polarization down to the monolayer limit [2], metal-insulator transitions [3], tunable Weyl and Dirac states [4], and Rashba states [5].

In practice it remains challenging to tune the polar buckling. One set of approaches is to use the substrate, via epitaxial strain or substrate templating. With epitaxial strain, substrate-induced changes in lattice parameter can tune polar distortions. Examples include strain induced ferroelectricity in $SrTiO_3$ [6, 7] and multiferroicity in $EuTiO_3$ [8, 9]. For substrate templating, intra-unit cell distortions of the substrate directly template the desired distortion in the film. An example is tuning octahedral tilts in transition metal oxide films by selecting a substrate with the desired tilt pattern [10, 11]. However, in these approaches the values of distortion are limited by the availability of substrates with the desired distortion pattern and lattice parameter.

Free-standing membranes are an attractive alternative due to the ability to continuously apply homogeneous strains and strain gradients. Bending of membranes has been theoretically proposed as a route for switching polar metals [12] and for tuning chiral spin textures via the Dzyaloshinskii-Moriya Interaction [13]. Recent experiments on single crystalline membranes of GdAuGe [14] and GdPtSb [15] demonstrate bending-induced changes in magnetic ordering, which may arise from changes in the AuGe or PtSb layer buckling. However, membrane control is still in its infancy and it remains challenging to control small radius of curvature bends repeatably and over large sample areas [16–18].

Here we use chemical pressure to continuously tune the polar buckling of *ABC* intermetallic films grown by molecular beam epitaxy (MBE) on (0001)-oriented Al_2O_3 substrates. Starting from LaPtSb, which is a high conductivity polar metal [19], we show that substitution of Gd for La reduces the interlayer spacing and increases the PtSb layer buckling by a factor of 2, due to the smaller atomic radius of Gd. The free carrier density decreases with x, the magnetic susceptibility peaks for small finite x, and the apparent Neel temperature increases with x. We interpret the magnetic trends with x in terms of RKKY coupling between local $4f$ moments, whose concentration increases with x, and the free carrier concentration that decreases with x.

II. RESULTS

We first use density functional theory (DFT) calculations to predict the structural distortions with Gd substitution and the corresponding changes to electronic structure. We focus on the end members LaPtSb and GdPtSb. Details of the computational methods are found in the Supplemental Materials.

Fig. 1(a) insert shows the crystal structure of LaPtSb, which experimentally crystallizes in the polar hexagonal LiGaGe-type structure (space group $P6_3mc$) [20]. Here the Pt and Sb form a distorted wurtzite-like sublattice. The buckling of the Pt-Sb planes, which we define as the displacement of Pt and Sb atoms along the c axis, breaks inversion symmetry and creates a unique polar axis along c. Our relaxed DFT calculations for LaPtSb predict a buckling of 35.1 pm and a c lattice parameter of 8.37 Å (Table 1 in the Supplemental Materials [21] (including references [22–28])). The corresponding electronic structure (without spin orbit coupling) is semimetallic with a band overlap of ~ 1 eV and primarily hole carriers (Fig. 1(e)).

GdPtSb experimentally crystallizes in the cubic half Heusler (space group $F\bar{4}3m$) with $abc-abc$ stacking [29], compared to the $ab-ab$ stacking of the hexagonal $P6_3mc$

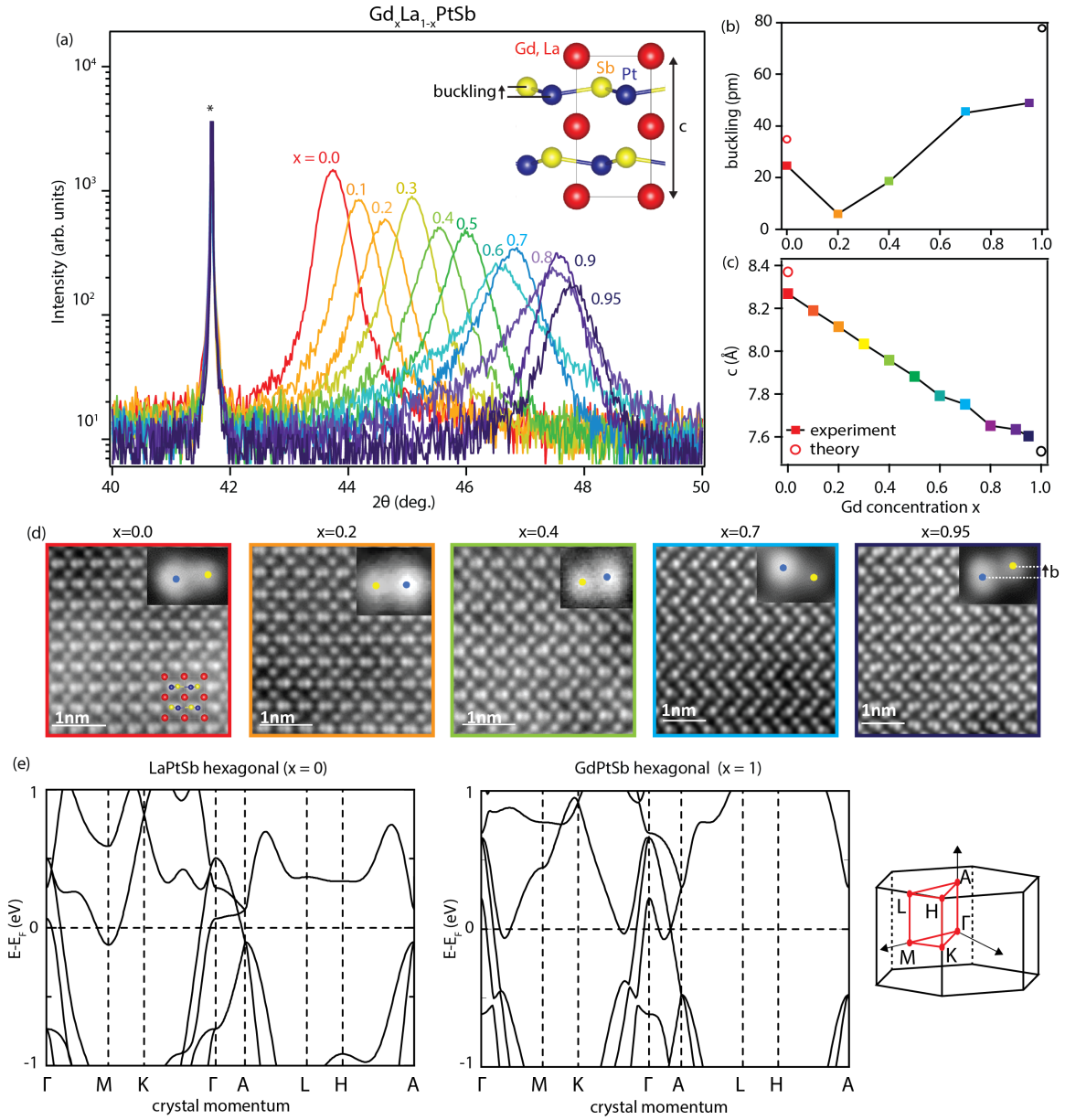

FIG. 1. (a) Symmetric $2\theta - \omega$ x-ray diffraction scans of the 0004 reflection. The asterisk marks an Al_2O_3 substrate reflection. Inset shows the crystal structure of *Ln*PtSb in the $P6_3mc$ structure with polar buckling of the PtSb planes. (b) PtSb layer buckling determined from Gaussian intensity fitting of the STEM intensity (closed squares), compared to DFT calculated buckling in the $P6_3mc$ structure (open circles). (c) Out of plane lattice parameter c determined from x-ray diffraction (closed squares), compared to DFT calculated lattice parameter in the $P6_3mc$ structure. (d) STEM images of samples with varying Gd composition x, measured along a $\langle 2\bar{1}\bar{1}0 \rangle$ zone axis. (e) DFT-GGA bandstructures of relaxed $P6_3mc$ LaPtSb and GdPtSb without SOC, and the corresponding $P6_3mc$ Brillouin zone.

structure (Supplemental Fig. 1(c,d)). To assess the maximum buckling anticipated for Gd-substituted LaPtSb, we compute the relaxed structure for GdPtSb in a hypothetical $P6_3mc$ structure. Our relaxed DFT calculations predict an enhanced buckling of 77.9 pm and a decreased c of 7.533 Å for GdPtSb. The corresponding electronic structure shows a smaller band overlaps than LaPtSb, including an increased band gap at A and an increase in the conduction band minima at M and H (Fig. 1(e)).

$Gd_xLa_{1-x}PtSb$ films with thickness 20-30 nm were grown by molecular beam epitaxy on Al_2O_3 (0001). This thickness was chosen such that the films are expected to fully relax to their bulk lattice parameter. The lattice mismatch between GdPtSb ($d_{110} = 4.72$ Å) and sapphire ($a = 4.758$ Å) is 2.4% tensile, and the lattice mismatch between LaPtSb ($a = 4.56$ Å) and sapphire is 4.3% tensile. These mismatches correspond to Matthews-Blakeslee critical thicknesses of order 1 nm. Details of MBE synthesis and x-ray diffraction (XRD) characterization appear in Supplemental Materials.

Wide angle $2\theta - \omega$ XRD scans show that our

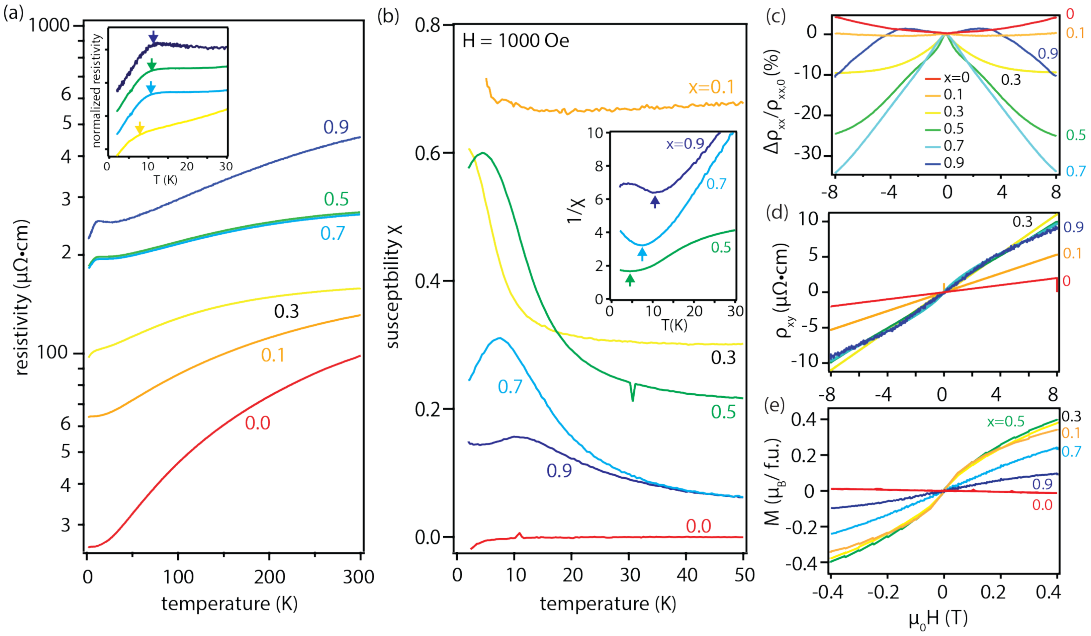

FIG. 2. (a) Resistivity ρ_{xx} versus temperature for films with varying Gd composition. Insert shows identification of T^* via a tangent construction. (b) Magnetic susceptibility $\chi \approx M/H$ measured at 1000 Oe with field oriented out of plane. (c) Magnetoresistance versus applied field at 2 K with field oriented out of plane and current in-plane. (d) Transverse (Hall) resistivity versus applied field at 2 K. (e) Magnetization versus applied field at 2 K with field out of plane.

$Gd_xLa_{1-x}PtSb$ films form a continuous solid solution from x = 0 to 1 with no secondary phases and retain the hexagonal structure out to $x \leq 0.95$ (Fig. 1(a) and Supplemental Fig. 1(a)). With increasing Gd composition x we observe an increase in the Bragg angle of the hexagonal 0004 reflection, corresponding to a decreasing out of plane lattice constant c (Fig. 1(c), filled squares). This experimental trend is in good agreement with our DFT calculations for LaPtSb and GdPtSb (Fig. 1(c) open circles and Table 1). We attribute the decreased c to the smaller ionic radius of Gd compared to La, due to the lanthanide contraction. The in-plane lattice parameters, extracted from off axis scans of the $10\bar{1}2$ reflections, show a much weaker dependence on x as they vary from 4.50 to 4.58 Å for $x \leq 0.95$. We attribute the large changes in c, and relatively weak changes in a, to the quasi-2D layered structure of the $P6_3mc$ (LiGaGe-type) structure [30]. In this bonding picture, the lanthanide cations behave as intercalants that "stuff" between polyanionic PtSb sheets.

We use off axis azimuthal ϕ scans to distinguish cubic from hexagonal polymorphs. We find that the hexagonal structure is retained out to $x \leq 0.95$. These samples display a six-fold rotation of the $10\bar{1}2$ reflection corresponding to the hexagonal structure, whereas the $x = 1$ end member GdPtSb displays a three-fold rotation corresponding to cubic structure (Supplemental Fig. 1(b)). The hexagonal $10\bar{1}2$ film reflections for $x \leq 0.95$ align in ϕ with the $10\bar{1}4$ reflections of the sapphire substrates, corresponding to an epitaxial relationship of $Gd_xLa_{1-x}PtSb\ [10\bar{1}0](0001) \parallel Al_2O_3\ [10\bar{1}0](0001)$. For the $x = 1$ cubic sample, in addition to the three-fold 220 reflections that align with the sapphire $10\bar{1}4$, we observe a second set of weaker reflection that are rotated in ϕ by 60 degrees. We attribute this second set to an antiphase domain.

We quantify the buckling using high angle annular diffraction (HAADF) scanning transmission microscopy (STEM imaging, see Supplemental Materials). In Fig. 1(d) the brightest atomic columns correspond to Pt, next brightest to Gd/La, and lowest intensity to Sb. We observe hexagonal $ab-ab$ layer stacking for $x \leq 0.95$ (Fig. 1(d)) and cubic $abc-abc$ stacking for $x = 1$ (Supplemental Fig. 1(d)), consistent with the XRD ϕ scans. From 2D Gaussian fitting of the intensity we extract the polar buckling. We find an overall increase in the buckling with Gd composition x (Fig. 1(b)), consistent with our DFT calculations, which we attribute to stronger interlayer bonding with decreased c. Interestingly, we find that the buckling decreases going from $x = 0$ to $x = 0.2$, then monotonically increases with x. At this point the reason for the local minimum is unclear.

Temperature dependent resistivity ρ reveals a metal-like temperature dependence $d\rho/dT > 0$ for all samples and an increase in ρ with Gd composition (Fig. 2(a)). This is consistent with our DFT calculations that predict decreased band overlaps for GdPtSb compared with LaPtSb (Fig. 1(e)). Samples with intermediate Gd composition $0.3 \leq x \leq 0.9$ display kinks in the resistivity versus temperature at a temperature T^*, which we define by a local tangent construction (Supplemental Fig. 2). We attribute these kinks to magnetic phase transitions. The kinks correspond approximately, but not exactly, to kinks that we observe in the inverse of the magnetic susceptibility versus temperature (Fig. 2(b) insert).

The 2 K magnetoresistance is shown in Fig. 2(c). Samples with $x \leq 0.1$ show a weak positive quadratic dependence on

applied field. With increasing x we observe a more negative magnetoresistance, which we attribute to field alignment of $4f$ moments that suppresses free carrier scattering.

Hall effect measurements (Fig. 2(d)) show a positive sign indicating hole dominated transport. Samples with $x \leq 0.1$ show a linear ρ_{xy} vs applied field and are well fit to model with a single hole band. Samples with $x > 0.1$ show nonlinear behavior at low fields $\mu_0 H < 4$ T, which may arise from an anomalous Hall effect consistent with the nonlinear $M(H)$ measured by SQUID (Fig. 2(e)). For these samples we extract a hole density from a high field fit to the linear component of $\rho_{xy}(B)$ (Supplemental Fig. 3). The results of the Hall modelling are shown in Fig. 3(c), where we find a decrease in the hole density with increasing Gd composition. We attribute this decreasing carrier density to the increased Pt-Sb layer buckling, which decreases the bandwidths and band overlaps at the Fermi energy. The Gd $4f$ bands, which are located ~ 8 eV below the Fermi energy by DFT calculations, are not anticipated to contribute free carriers.

SQUID magnetometry measurements at 2 K show that LaPtSb is diamagnetic with a negative and linear M vs applied field H (Fig. 2(e)). For $0.1 \leq x \leq 0.5$, we observe a positive nonlinear dependence of $M \propto \tanh(H)$ with no clear hysteresis, suggestive of superparagmagnetism from dilute Gd $4f$ moments or clusters of $4f$ moments. For $x \geq 0.7$ we observe a linear positive $M(H)$. Fig. 2(b) shows the temperature dependent magnetic susceptibility, which we define as M/H at low field H = 1000 Oe. For samples with $x \geq 0.5$ we observe a negative Curie-Weiss temperature (Fig. 2(b) insert), consistent with antiferromagnetic transitions. The apparent Neel transition temperature versus Gd composition is shown in Fig. 3(a). Whereas GdPtSb is anticipated to be a G-type antiferromagnet [15] consistent with the ordering of GdPtBi [31], the spin structure of $Gd_xLa_{1-x}PtSb$ for $x < 1$ is not known and requires further study.

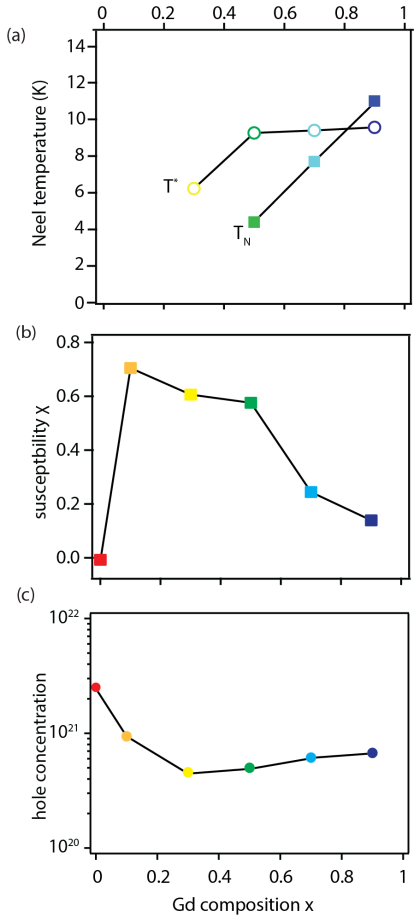

FIG. 3. (a) Neel temperature T_N extracted from kink in $1/\chi$ versus T (filled squares) and T^* extracted from the knink in $\rho(T)$ (open circles). (b) Magnetic susceptibility at 2 K, defined as M/H at $H =$ 1000 Oe. (c) Carrier concentration extracted from Hall effect using a single band model.

III. DISCUSSION

We summarize the key trends of magnetism and transport with Gd composition x in Fig. 3. Fig. 3(a) plots the characteristic temperatures: T^* from kink in $\rho(T)$ and the Neel temperature T_N from the kink in the inverse of magnetic susceptibility versus temperature. Both characteristic temperatures increase monotonically with Gd composition, which we attribute to the increasing concentration of Gd $4f$ moments. We find that T_N and T^* are close, but do not exactly coincide. The difference in T^* and T_N may be due to an intermediate magnetic state, since other lanthanide-containing ABC compounds display multiple transitions due to magnetic frustration [32].

We caution, however, that instead of kinks in $\rho(T)$, magnetic transitions observed by transport measurements are more formally related to anomalies in the derivative $d\rho/dT$ [33]. In particular, in the limit of small Fermi wavenumber k_F the magnetic transition temperature corresponds to the peak in $d\rho/dT$ [33]. However, this simple relationship rapidly breaks down for larger k_F. Our DFT calculations suggest that hexagonal $Gd_xLa_{1-x}PtSb$ has large k_F (Fig. 1(e)), consistent with the large carrier density that we observe by Hall effect (Fig. 2(d) and Fig. 3). The resulting experimental $d\rho/dT$ curves display broad minima in which it is difficult to define a clear transition temperature (Supplemental Fig. 2). Therefor in our data we find that the tangent construction of T^* provides a more clearly defined transition.

The hole concentration extracted from Hall effect at 2 K decreases with Gd composition (Fig. 3c). We attribute this trend to the increase in c lattice parameter with x, which decreases the intralayer hoppings and decreases the band overlap at the Fermi energy.

The magnetic susceptibility χ dependence on x is more complex: starting from a small negative value for diamagnetic LaPtSb at $x = 0$, the susceptibility rapidly peaks for $x = 0.1$ and then gradually decreases (Fig. 3b). We interpret the non monotonic trend in χ to arise from the Ruderman–Kittel–Kasuya–Yosida (RKKY) interaction [34, 35] in which local Gd $4f$ are coupled via the Fermi sea. With increasing x the concentration of Gd $4f$ moments increases; however, the concentration of hole carrier decreases due to the layer buckling. This causes the peak susceptibility to occur

at an intermediate Gd concentration. The peak in $\chi(x)$ corresponds to the samples that show superparamagnetic $M(H)$ at low Gd concentration ($x \leq 0.5$). For larger values of Gd concentration $x > 0.5$, as the Gd moments are closer together, the RKKY coupling is antiferromagnetic resulting in a linear $M(H)$ and a rapid decrease in susceptibility with increasing Gd composition.

In conclusion, we demonstrated epitaxial synthesis of $Gd_xLa_{1-x}PtSb$ films on Al_2O_3 (0001) with highly tunable polar buckling that is 2 times larger than the buckling for LaPtSb. The hole concentration decreases with Gd-induced layer buckling. Gd substitution also contributes local $4f$ moments, which order antiferromagnetically for high concentrations x. We explain the magnetic susceptibility in terms of a competition between Pt-Sb buckling that decreases the hole concentration, versus an increase in the concentration of Gd $4f$ moments in an RKKY picture. The lanthanide substituted *ABC* intermetallics offer a continuously tunable platform for exploring the effects of polar distortions on magnetism in a $4f$ system.

IV. ACKNOWLEDGMENT

Transport and magnetometry by JKK and DD were supported by the Air Force Office of Scientific Research (FA9550-21-0127) and by the Army Research Office (W911NF-17-1-0254). Epitaxial synthesis by DD and JKK was supported by the U.S. Department of Energy (DE-SC0023958). Data analysis and writing of the manuscript by all authors were supported in part by the National Science Foundation via the Wisconsin Materials Research Science and Engineering Center (MRSEC, DMR-2309000). DFT calculations by KMR, KG, and YT were supported by ONR grant N00014-21-1-2107. STEM measurements by CZ, JW, and PMV were supported by the NSF through the University of Wisconsin Materials Research Science and Engineering Center (DMR-2309000). We gratefully acknowledge use of facilities and instrumentation supported by NSF through the University of Wisconsin Materials Research Science and Engineering Center (DMR-2309000).

[1] J. W. Bennett, K. F. Garrity, K. M. Rabe, and D. Vanderbilt, "Hexagonal a b c semiconductors as ferroelectrics," *Physical review letters*, vol. 109, no. 16, p. 167602, 2012.

[2] K. F. Garrity, K. M. Rabe, and D. Vanderbilt, "Hyperferroelectrics: proper ferroelectrics with persistent polarization," *Physical review letters*, vol. 112, no. 12, p. 127601, 2014.

[3] K. T. Genser, *First principles investigations of structures and properties of ternary ABC compounds in hexagonal and Half-Heusler configurations*. PhD thesis, Rutgers University-School of Graduate Studies, 2024.

[4] H. Gao, Y. Kim, J. W. Venderbos, C. Kane, E. Mele, A. M. Rappe, and W. Ren, "Dirac-weyl semimetal: Coexistence of dirac and weyl fermions in polar hexagonal a b c crystals," *Physical Review Letters*, vol. 121, no. 10, p. 106404, 2018.

[5] D. Di Sante, P. Barone, A. Stroppa, K. F. Garrity, D. Vanderbilt, and S. Picozzi, "Intertwined rashba, dirac, and weyl fermions in hexagonal hyperferroelectrics," *Physical review letters*, vol. 117, no. 7, p. 076401, 2016.

[6] J. Haeni, P. Irvin, W. Chang, R. Uecker, P. Reiche, Y. Li, S. Choudhury, W. Tian, M. Hawley, B. Craigo, *et al.*, "Room-temperature ferroelectricity in strained srtio3," *Nature*, vol. 430, no. 7001, pp. 758–761, 2004.

[7] D. G. Schlom, L.-Q. Chen, C.-B. Eom, K. M. Rabe, S. K. Streiffer, and J.-M. Triscone, "Strain tuning of ferroelectric thin films," *Annu. Rev. Mater. Res.*, vol. 37, no. 1, pp. 589–626, 2007.

[8] J. H. Lee, L. Fang, E. Vlahos, X. Ke, Y. W. Jung, L. F. Kourkoutis, J.-W. Kim, P. J. Ryan, T. Heeg, M. Roeckerath, *et al.*, "A strong ferroelectric ferromagnet created by means of spin–lattice coupling," *Nature*, vol. 466, no. 7309, pp. 954–958, 2010.

[9] C. J. Fennie and K. M. Rabe, "Magnetic and electric phase control in epitaxial eutio 3 from first principles," *Physical review letters*, vol. 97, no. 26, p. 267602, 2006.

[10] J. M. Rondinelli, S. J. May, and J. W. Freeland, "Control of octahedral connectivity in perovskite oxide heterostructures: An emerging route to multifunctional materials discovery," *MRS bulletin*, vol. 37, no. 3, pp. 261–270, 2012.

[11] Y. Yang, C. M. Schlepütz, C. Adamo, D. G. Schlom, and R. Clarke, "Untilting bifeo3: The influence of substrate boundary conditions in ultra-thin bifeo3 on srtio3," *APL Materials*, vol. 1, no. 5, 2013.

[12] A. Zabalo and M. Stengel, "Switching a polar metal via strain gradients," *Physical Review Letters*, vol. 126, no. 12, p. 127601, 2021.

[13] Y. Ga, Q. Cui, J. Liang, D. Yu, Y. Zhu, L. Wang, and H. Yang, "Dzyaloshinskii-moriya interaction and magnetic skyrmions induced by curvature," *Physical Review B*, vol. 106, no. 5, p. 054426, 2022.

[14] Z. LaDuca, T. Samanta, N. Hagopian, T. Jung, K. Su, K. Genser, K. M. Rabe, P. M. Voyles, M. S. Arnold, and J. K. Kawasaki, "Cold seeded epitaxy and flexomagnetism in gdauge membranes exfoliated from graphene/ge (111)," *Nano Letters*, vol. 24, no. 33, pp. 10284–10289, 2024.

[15] D. Du, S. Manzo, C. Zhang, V. Saraswat, K. T. Genser, K. M. Rabe, P. M. Voyles, M. S. Arnold, and J. K. Kawasaki, "Epitaxy, exfoliation, and strain-induced magnetism in rippled heusler membranes," *Nature communications*, vol. 12, no. 1, p. 2494, 2021.

[16] O. G. Schmidt and K. Eberl, "Thin solid films roll up into nanotubes," *Nature*, vol. 410, no. 6825, pp. 168–168, 2001.

[17] D.-H. Kang, H. Sun, M. Luo, K. Lu, M. Chen, Y. Kim, Y. Jung, X. Gao, S. J. Parluhutan, J. Ge, *et al.*, "Pseudo-magnetic field-induced slow carrier dynamics in periodically strained graphene," *Nature Communications*, vol. 12, no. 1, p. 5087, 2021.

[18] D. Du, J. Hu, and J. K. Kawasaki, "Strain and strain gradient engineering in membranes of quantum materials," *Applied Physics Letters*, vol. 122, no. 17, 2023.

[19] D. Du, A. Lim, C. Zhang, P. J. Strohbeen, E. H. Shourov, F. Rodolakis, J. L. McChesney, P. Voyles, D. C. Fredrickson, and J. K. Kawasaki, "High electrical conductivity in the epitaxial polar metals laauge and laptsb," *APL Materials*, vol. 7, no. 12, p. 121107, 2019.

[20] R.-D. Hoffmann and R. Pöttgen, "Alb2-related intermetallic compounds–a comprehensive view based on group-subgroup

relations," *Zeitschrift für Kristallographie-Crystalline Materials*, vol. 216, no. 3, pp. 127–145, 2001.

[21] "See supplemental material at [url will be inserted by publisher] for experimental and computational methods, extended structural and transport data, and extended dft calculations.,"

[22] A. B. Yankovich, B. Berkels, W. Dahmen, P. Binev, S. I. Sanchez, S. A. Bradley, A. Li, I. Szlufarska, and P. M. Voyles, "Picometre-precision analysis of scanning transmission electron microscopy images of platinum nanocatalysts," *Nature communications*, vol. 5, no. 1, p. 4155, 2014.

[23] G. Kresse and J. Hafner, "Ab initio molecular dynamics for liquid metals," *Phys. Rev. B*, vol. 47, pp. 558–561, 1 1993.

[24] G. Kresse and J. Furthmüller, "Efficient iterative schemes for ab initio total-energy calculations using a plane-wave basis set," *Phys. Rev. B*, vol. 54, pp. 11169–11186, 10 1996.

[25] J. P. Perdew, K. Burke, and M. Ernzerhof, "Generalized gradient approximation made simple [phys. rev. lett. 77, 3865 (1996)]," *Phys. Rev. Lett.*, vol. 78, pp. 1396–1396, 2 1997.

[26] P. E. Blöchl, "Projector augmented-wave method," *Phys. Rev. B*, vol. 50, pp. 17953–17979, 12 1994.

[27] M. Methfessel and A. T. Paxton, "High-precision sampling for brillouin-zone integration in metals," *Phys. Rev. B*, vol. 40, pp. 3616–3621, Aug 1989.

[28] V. Wang, N. Xu, J.-C. Liu, G. Tang, and W.-T. Geng, "Vaspkit: A user-friendly interface facilitating high-throughput computing and analysis using vasp code," *Computer Physics Communications*, vol. 267, p. 108033, 2021.

[29] D. Du, L. R. Thoutam, K. T. Genser, C. Zhang, K. M. Rabe, T. Samanta, T. Jung, B. Jalan, P. M. Voyles, and J. K. Kawasaki, "Effect of pt vacancies on magnetotransport of weyl semimetal candidate gdptsb epitaxial films," *Physical Review Materials*, vol. 7, no. 8, p. 084204, 2023.

[30] F. Casper, C. Felser, R. Seshadri, C. P. Sebastian, and R. Pöttgen, "Searching for hexagonal analogues of the half-metallic half-heusler xyz compounds," *Journal of Physics D: Applied Physics*, vol. 41, no. 3, p. 035002, 2008.

[31] T. Suzuki, R. Chisnell, A. Devarakonda, Y.-T. Liu, W. Feng, D. Xiao, J. W. Lynn, and J. Checkelsky, "Large anomalous hall effect in a half-heusler antiferromagnet," *Nature Physics*, vol. 12, no. 12, pp. 1119–1123, 2016.

[32] D. Ram, J. Singh, M. Hooda, K. Singh, V. Kanchana, D. Kaczorowski, and Z. Hossain, "Multiple magnetic transitions, metamagnetism, and large magnetoresistance in gdauge single crystals," *Physical Review B*, vol. 108, no. 23, p. 235107, 2023.

[33] M. E. Fisher and J. Langer, "Resistive anomalies at magnetic critical points," *Physical Review Letters*, vol. 20, no. 13, p. 665, 1968.

[34] M. A. Ruderman and C. Kittel, "Indirect exchange coupling of nuclear magnetic moments by conduction electrons," *Physical Review*, vol. 96, no. 1, p. 99, 1954.

[35] T. Kasuya, "A theory of metallic ferro-and antiferromagnetism on zener's model," *Progress of theoretical physics*, vol. 16, no. 1, pp. 45–57, 1956.